THE ASTRONOMICAL JOURNAL VOLUME 113, NUMBER 2 FEBRUARY 1997

NEW H I OBSERVATIONS OF THE PROTOTYPE POLAR RING GALAXY NGC 4650A[1]

M. ARNABOLDI
Mount Stromlo and Siding Spring Observatories, Canberra, Australia
Electronic mail: magda@mso.anu.edu.au

T. OOSTERLOO
Australia Telescope National Facility–CSIRO, Sydney, Australia
Electronic mail: toosterl@atnf.csiro.au

F. COMBES
Observatoire de Paris Meudon, DEMIRM, Paris, France
Electronic mail: bottaro@mesioa.obspm.fr

K. C. FREEMAN
Mount Stromlo and Siding Spring Observatories, Canberra, Australia
Electronic mail: kcf@mso.anu.edu.au

B. KORIBALSKI
Australia Telescope National Facility–CSIRO, Sydney, Australia
Electronic mail: bkoribal@atnf.csiro.au

Received 1996 June 19; revised 1996 October 17

ABSTRACT

New, high resolution observations of the H I emission line and 20-cm continuum at the Australia Telescope Compact Array (ATCA) for the prototype polar ring galaxy NGC 4650A are presented. We show the presence of a far more extended H I distribution than previously observed with the VLA, and a very regular velocity field out to a distance of ~50 kpc. The combined analysis of the H I data with optical and near-infrared images argues against previous warp models used to describe the dynamics of this object. A comparison between the high resolution H I images and a new B-band image obtained at the ESO NTT further weakens the interpretation of the optical morphology via warp geometries. The presence of two spiral arms stretching out in the polar disk seems to represent the most likely explanation for the observed morphology and kinematics. © *1997 American Astronomical Society.* [S0004-6256(97)03001-X]

1. INTRODUCTION

Polar ring (PR) galaxies have been the target for several attempts to constrain the shape of dark matter halos: e.g., Schweizer *et al.* 1983, Whitmore *et al.* 1987 (WMS), Sackett & Sparke 1990 (SS), Sackett *et al.* 1994 (S94). They are early-type galaxies, ellipticals or S0, with a ring or annulus of gas, stars, and dust orbiting in a plane nearly perpendicular to the equatorial plane of the host galaxy. The presence of mass tracers in two roughly perpendicular planes gives an opportunity to determine the 3D shape of the dark matter distribution. In particular, the prototype polar ring galaxy NGC 4650A has motivated numerous efforts (Lausten & West 1980; WMS; SS; S94) in the difficult task to obtain limits on the dark halo shape.

So far the results have been contradictory. WMS compared the optical rotational speeds in the equatorial and polar planes at a distance of ~ 0.6 R_{25} in NGC 4650A, and concluded that the dark matter halo was nearly spherical. The same optical data were analyzed by SS in a more detailed study using a physically realistic potential that included the effects of luminous components and compared the predicted model to the entire extent of both equatorial and polar rotation curves. SS showed that a range of dark halo flattenings from E0 to E8 were compatible with the data; their best fit was E5, and the spherical case gave a relatively poor fit. Recently, S94 proposed a dynamical model for NGC 4650A using new optical observations of the radial velocities and velocity dispersion for the host S0 galaxy, which rules out the spherical halo option. Their best fit model includes a dark halo with an E6 to E7 flattening, with the dark matter distribution axes aligned with those of the S0 disk. Arnaboldi *et al.* (1993) also favored a flattened dark matter halo for AM 2020−504, the only known example of a polar ring around an elliptical galaxy. The best fit was found for a flattening equal to that of the projected light. In all these studies the dynamical models were compared with the optical rotation curves only.

There are intrinsic difficulties in the determination of the

[1]Based on observations made with the Australia Telescope Compact Array, Narrabri, NSW Australia, and at the European Southern Observatory, La Silla, Chile.

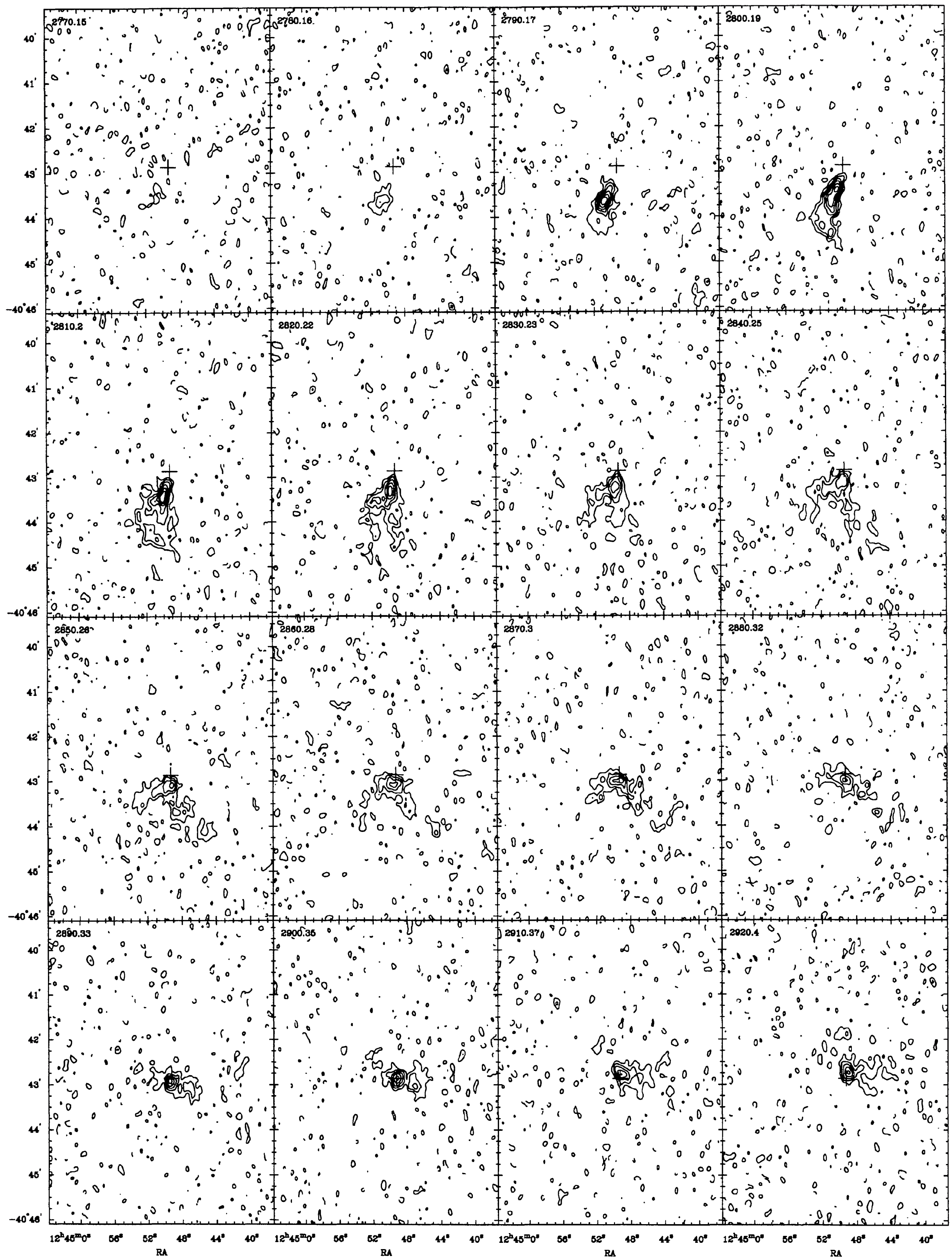

FIG. 1. Channel maps for the H I emission in NGC 4650A from 2770 to 3040 km s^{-1}, in steps of 10 km s^{-1}; the systemic velocity is at 2905 km s^{-1}. Dashed lines indicate contours at -1.6 mJy beam^{-1}, continuous-lines contours from 1.6 mJy beam^{-1} (2σ) in steps of 0.7 mJy beam^{-1}. The size of the synthesized beam is $12'' \times 9''$ with P.A.=0.8°.

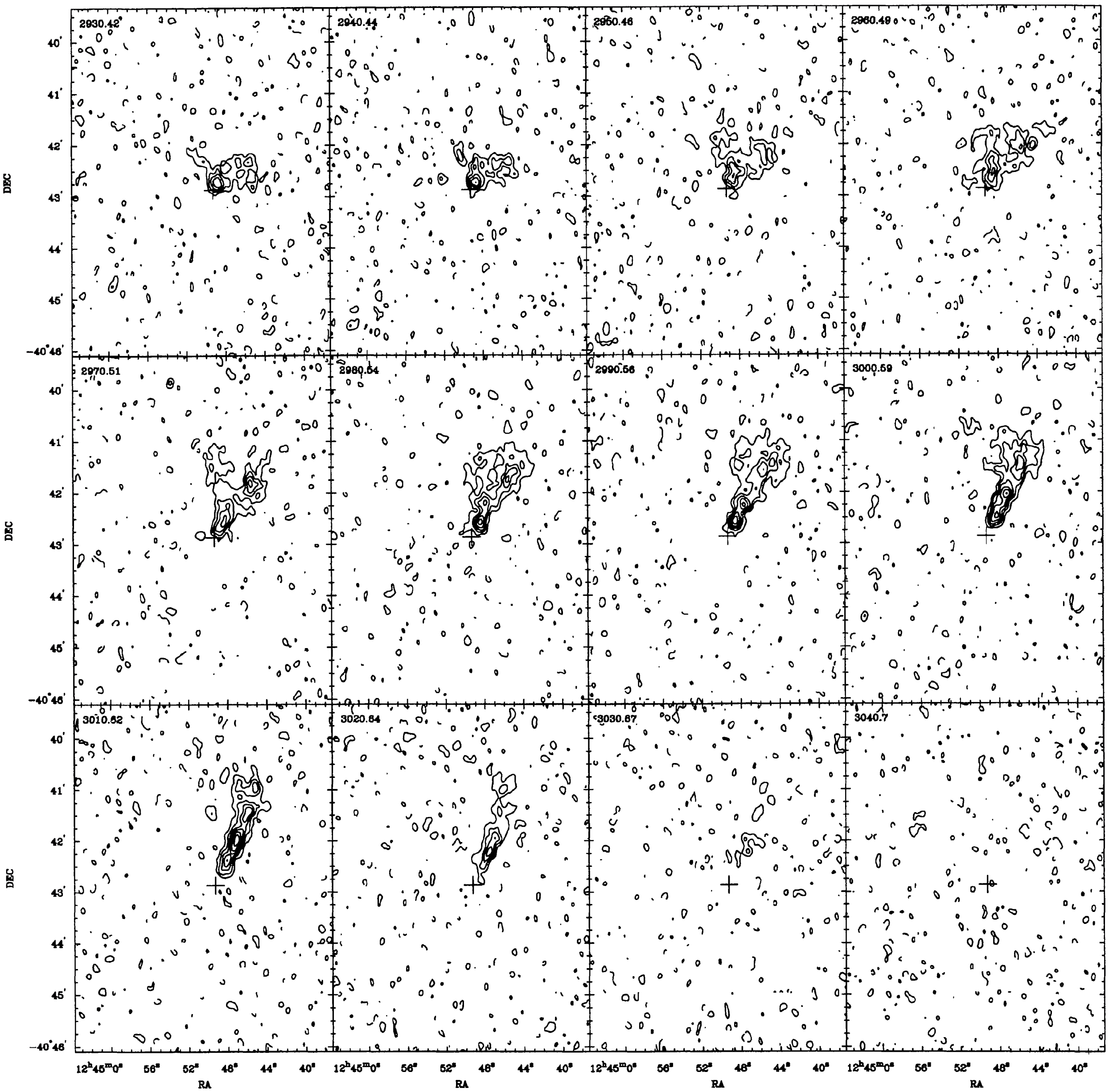

FIG. 1. (continued)

shape of the dark component: as emphasized by Reshetnikov & Combes (1994) polar ring galaxies may give only an indirect measure of the halo shape, because the method is based on extrapolation of the inner mass model, determined mainly by the luminous mass, into the outer polar region, where the dynamical information comes from the polar ring H I gas.

A recent dynamical model proposed by Combes & Arnaboldi (1996) indicates that the kinematics of the polar ring galaxy NGC 4650A within a radius of 100″ can be accounted for in the two orthogonal planes by the luminous component alone: dark matter is only needed to account for the polar ring kinematics traced by the H I gas observed by Van Gorkom *et al.* (1987; hereafter vGSK87) at large distances from the galaxy center. This result is very similar to the situation observed for late-type spirals; again, the luminous component completely accounts for the observed rotation in the inner regions (Kent 1986, 1987), while the dark halo is needed to explain the kinematics in the far outer regions. The similarity between spirals and the wide polar rings of S0 systems is strengthened by a recent study of the *BRK* broad band photometry for a sample of polar ring galaxies (Arnaboldi *et al.* 1995). This survey shows (i) a color gradient in the polar annuli towards bluer colors at larger radii, very similar to the observed color gradients of the late-type spiral disks (Kent 1992; de Jong & van der Kruit 1994); and (ii) integrated $B-R$, $R-K$ colors of PRs are very similar to those of spirals.

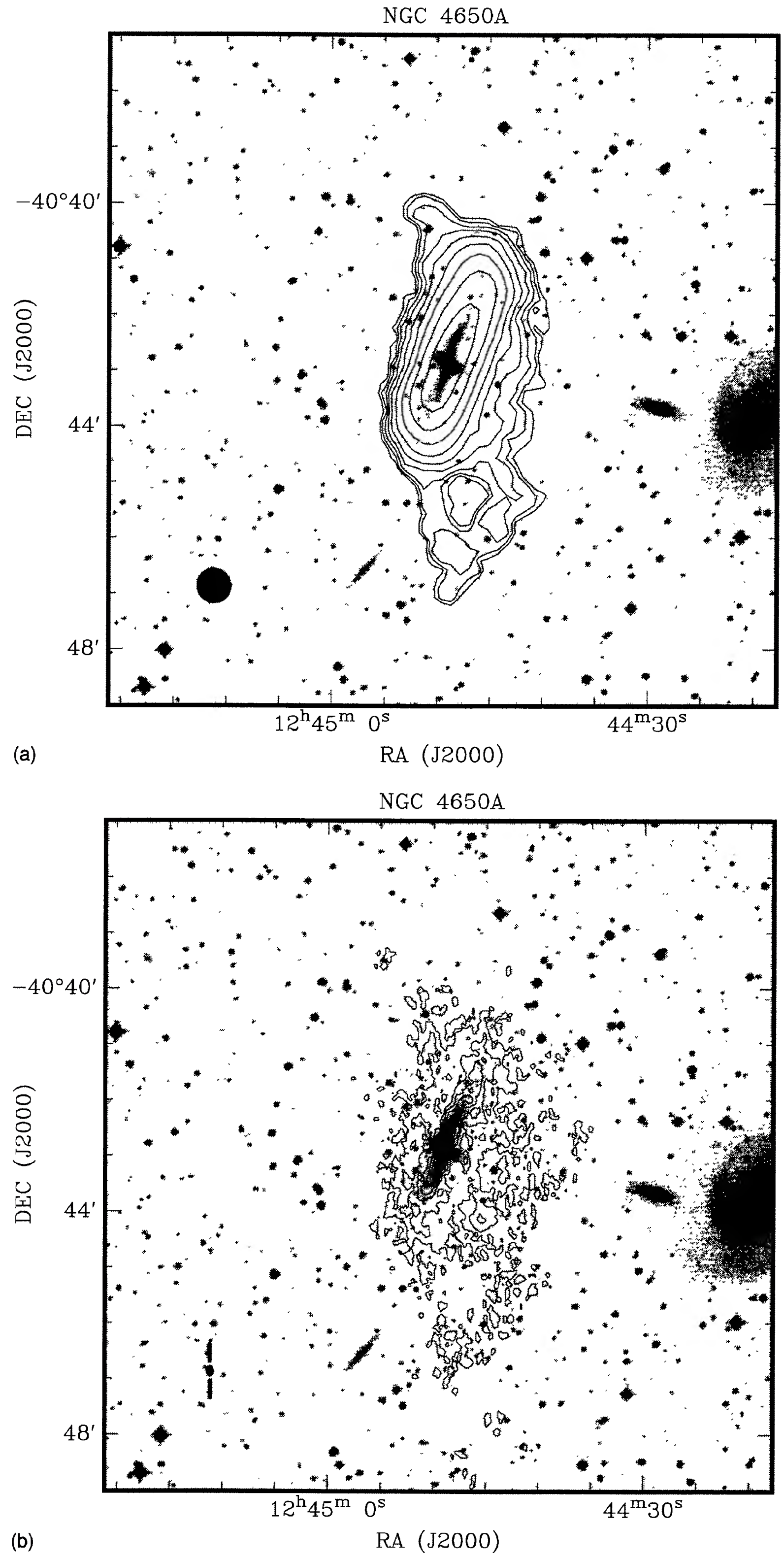

FIG. 2. (a) Contours of H I column density for NGC 4650A from the low resolution data cube superposed on the DSS image. Contours are drawn on a logarithmic scale from 5×10^{19} atoms cm^{-2} or $M_{\odot}$ pc^{-2}, in steps of 0.204 in the log. The size of the half-power synthesized beam is 39″×38″ with P.A.=27.8°, and is shown by the shaded ellipse. (b) Contours of H I column density for NGC 4650A from the high resolution data cube superposed on the DSS image. Contours are drawn from 1.6×10^{20} atoms cm^{-2} or 1.26 $M_{\odot}$ pc^{-2} in step of 1.6×10^{21} atoms cm^{-2} or 12.6 $M_{\odot}$ pc^{-2}. The size of the synthesized beam is 12″×9″ with P.A.=0.8°, and is shown by the small shaded ellipse in the lower left corner.

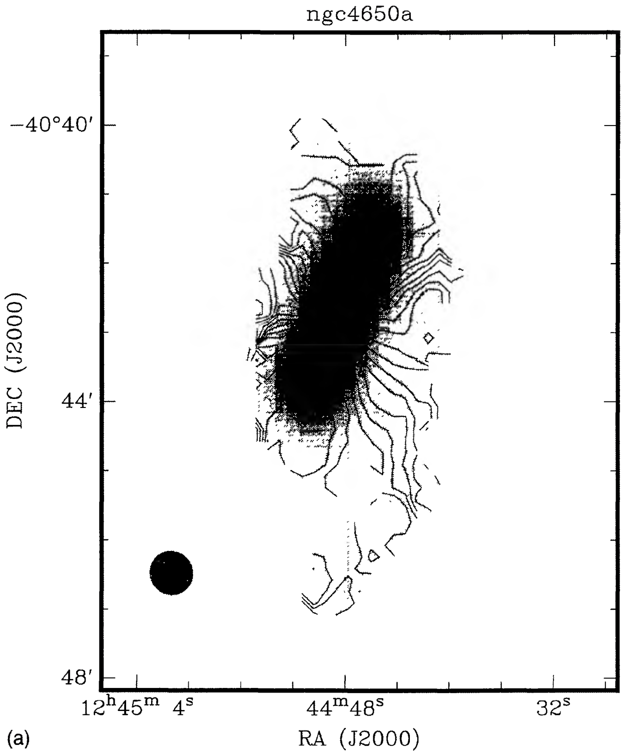

(a)

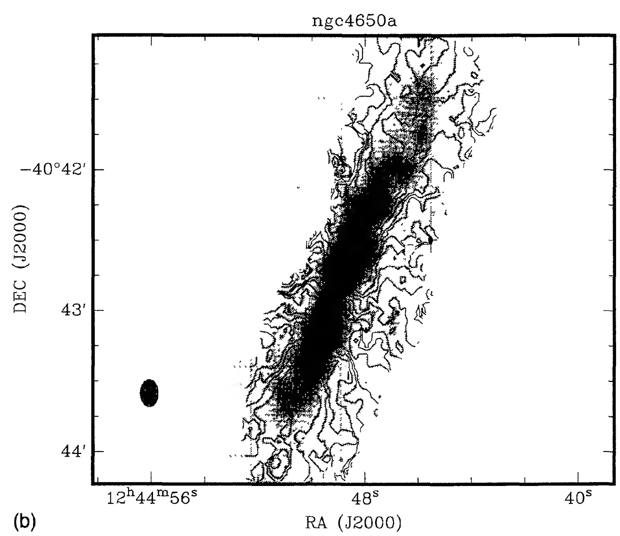

(b)

FIG. 3. (a) Low resolution 2D velocity field superposed on the H I distribution (grey-scale level); iso-velocity contours are drawn in steps of 10 km s^{-1}. (b) High resolution 2D velocity field superposed on the H I distribution (grey-scale level); iso-velocity contours are drawn in step of 10 km s^{-1}. The systemic velocity contour (2905 km s^{-1}) is coincident with the center of the S0.

In spiral galaxies, there is evidence that the dark matter surface density distribution is proportional to the H I distribution (see Freeman 1993). In the PR galaxy NGC 4650A, the H I lies entirely in the polar ring (vGSK87). This led Combes and Arnaboldi to try a dynamical model for NGC 4650A in which the dark component is flattened with the same axes as the polar ring itself. In this model, the dark matter distribution is simply taken to be proportional to the H I gas distribution in the NGC 4650A system, just as it appears to be in spiral galaxies. The model was able to reproduce the observed kinematics in the optical region and the relatively low angular resolution H I velocity field by vGSK87. The derived ratio between the dark matter surface density and the H I surface density is ~10, similar to the ratio measured in spiral galaxies (e.g., Bosma 1981; Freeman 1993) and the H I-rich dwarf irregulars (e.g., Carignan & Freeman 1988).

Because this question of the dark halo shape is so important as a test of cosmological simulations, the Combes-Arnaboldi hypothesis to explain the dynamics of NGC

TABLE 1. Comparison of VLA and ATCA observations.

	VLA	ATCA
Total integration time	4 hrs (DnC)	3×12 hrs (1.5B,C+6C)
	7 hrs (BnC only)	
Neutral hydrogen (H I)		
velocity channel spacing	42 km s^{-1} (L)	10 km s^{-1} (L)
	21 km s^{-1} (H)	"(H)
synthesized beam	40″×30″ (L)	38″×39″ (L)
	20″×20″ (H)	9″×12″ (H)
rms noise/channel	1.3 mJy beam^{-1} (L)	1.1 mJy beam^{-1} (L)
	1.1 mJy beam^{-1} (H)	0.8 mJy beam^{-1} (H)
H I velocity range	2780–3040 km s^{-1}	2770–3040 km s^{-1}
H I systemic velocity	2910 km s^{-1}	2905 kn s^{-1}
H I rotation velocity	100 km s^{-1}	120 km s^{-1}
H I flux density	[16 Jy km s^{-1}]^3	23 Jy km s^{-1}
H I mass	46×10^8 M$_\odot$	80×10^8 M$_\odot$
Continuum		
bandwidth	3 MHz (=15×0.2 MHz)	128 MHz
synthesized beam		15″×15″
rms noise	~1.5 mJy beam^{-1}	0.05 mJy beam^{-1}
int. 20-cm flux	<3σ beam^{-1}	5.4 mJy total

(L)Low resolution H I data cube.
(H)High resolution H I data cube.
(3)This is an estimated flux: vGSK87 reported only a total mass for the neutral hydrogen from which the flux is computed assuming $H_0 = 100$ km s^{-1} Mpc^{-1}.

4650A needs further examination. This requires high angular resolution H I data. High resolution velocity fields obtained for systems with wide polar annuli may give us the opportunity to discriminate between (i) the conventional model of dark matter aligned with the parent S0 or (ii) dark matter spatially related to the gaseous component. If high resolution velocity fields confirm that the dark matter in polar ring systems is related to the ring itself, then this will be also an indirect test of the nature of dark matter, in the sense of the Pfenniger *et al.* (1994), and Pfenniger & Combes (1994) hypothesis.

To target these questions we obtained radio synthesis observations with the Australia Telescope Compact Array (ATCA) in the 21-cm line of neutral hydrogen for the polar ring galaxy NGC 4650A, and a new B-band image at the European Southern Observatory (ESO) New Technology Telescope (NTT). Details of our observations and reduction procedures are described in Sec. 2. Results from the observations, in the form of total H I distribution, H I mean velocity field, position-velocity diagrams, and H I channel maps are presented in Sec. 3. In Sec. 4, we discuss the implications of the high resolution H I data on previous warp models used to reproduce the morphology of the polar ring. We analyze in detail the failure of the models to reproduce the properties of the new H I data, and the optical and near-infrared images of NGC 4650A, and present possible alternatives. Conclusions are derived in Sec. 5. We assume a distance to NGC 4650A of 38 Mpc ($H_0 = 75$ km s^{-1} Mpc^{-1}; 1″=190 pc).

2. OBSERVATIONS AND DATA REDUCTION

2.1 21-cm Observations

The H I observations were carried out in 1995 April–May with the ATCA in the 1.5B, 1.5C, and 6C configurations. The integration time for each configuration was 12 hrs. We observed with a 8 MHz bandwidth in 512 channels, centered at a frequency of 1407 MHz (corresponding to 2830 km s^{-1}); unfortunately this band included a narrow interference spike at 1408 MHz. The channel affected by this interference was flagged and the data were Hanning smoothed to suppress the effects of the spectral ringing. Simultaneously with the line data, broadband data was recorded with a bandwidth of 128 MHz in 32 channels, centered on 1380 MHz.

The data were calibrated with the standard ATCA procedures using the MIRIAD environment (Sault *et al.* 1995). The data were flux- and bandpass-calibrated using observations of PKS 1934−638 for which we adopted a flux of 14.96 Jy at 1380 MHz and 14.87 Jy at 1413 MHz. The continuum emission was subtracted from the visibility data using a linear fit to the line-free parts of the spectrum. Two cubes were produced from the data, one low resolution cube using a

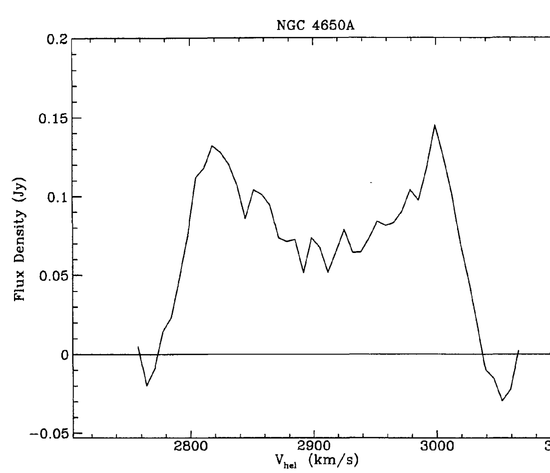

FIG. 4. Global H I profile for NGC 4650A.

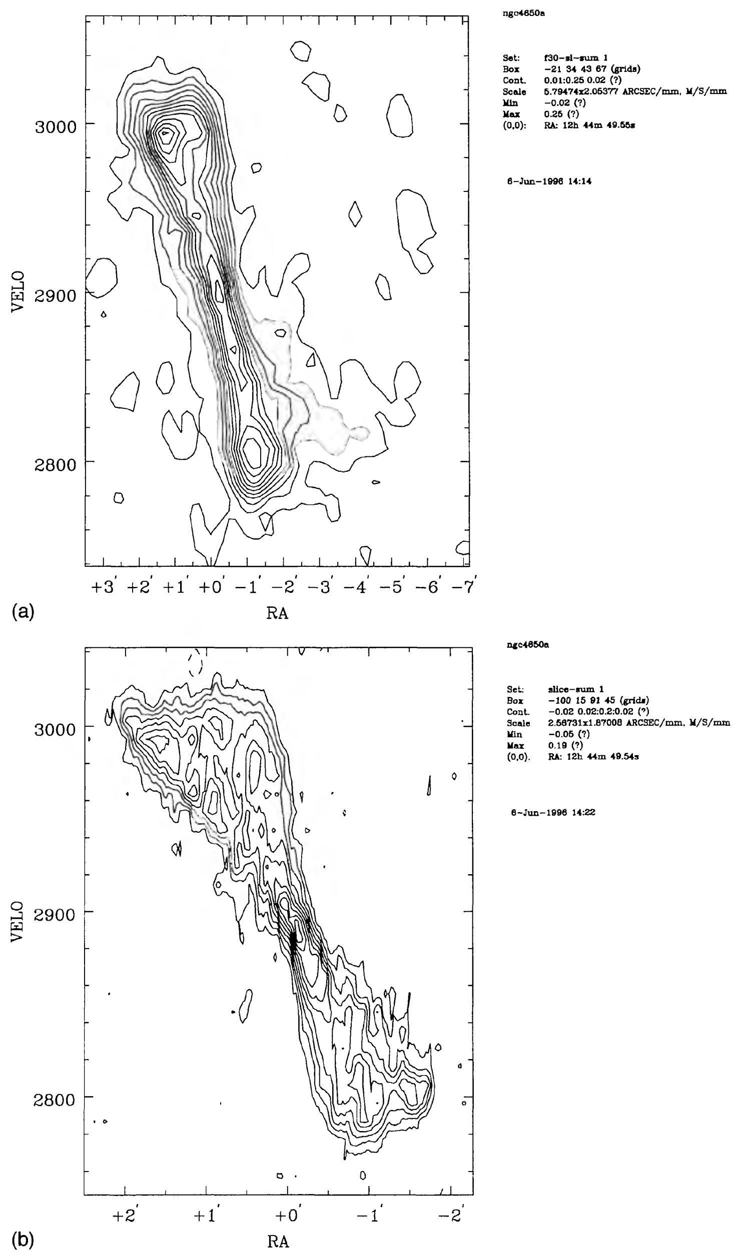

FIG. 5. (a) Position-velocity diagram along P.A.=158° for the H I low resolution data cube: the velocity tail related to the SW arch is clearly visible. Continuous lines indicate contours from 0.01 to 0.25 Jy beam^{-1} in steps of 0.02 Jy beam^{-1}. (b) Position-velocity diagram along P.A.=158° for the H I high resolution data cube; dashed lines indicate contour at −0.02 Jy beam^{-1}, continuous lines indicate contours from 0.02 to 0.2 Jy beam^{-1} in steps of 0.02 Jy beam^{-1}.

taper of 30″ (final FWHM resolution 38″×39″) and a high resolution cube without any taper (resolution 9″×12″). Both cubes were made using robust weighting (Briggs 1995) with robustness set at 0.3. This gives a weighting intermediate between uniform and natural weighting. We choose a channel width of 10 km s^{-1}. The noise in each channel map of the high resolution data is 0.8 mJy beam^{-1}; in the low resolution cube it is 1.1 mJy beam^{-1}. The resulting line cubes were further processed (CLEAN and moment analysis) using GIPSY (van der Hulst *et al.* 1992). Our radio continuum map gives a total flux for NGC 4650A of 5.4 mJy.

The mask for the construction of the low resolution H I distribution maps and velocity fields was created by (1) smoothing the low resolution cube spatially to a 60″×60″ beam, (2) introducing an additional Hanning smoothing in the velocities, and (3) using only the data in those pixels that were above 3 mJy beam^{-1} in this smoothed cube. The H I distribution and velocity fields derived from the high resolution cube were created using a mask obtained by (1) smoothing the high resolution cube spatially to a 30″×30″ beam, (2) introducing an additional Hanning smoothing in the velocities, and (3) using only the data in those pixels that were

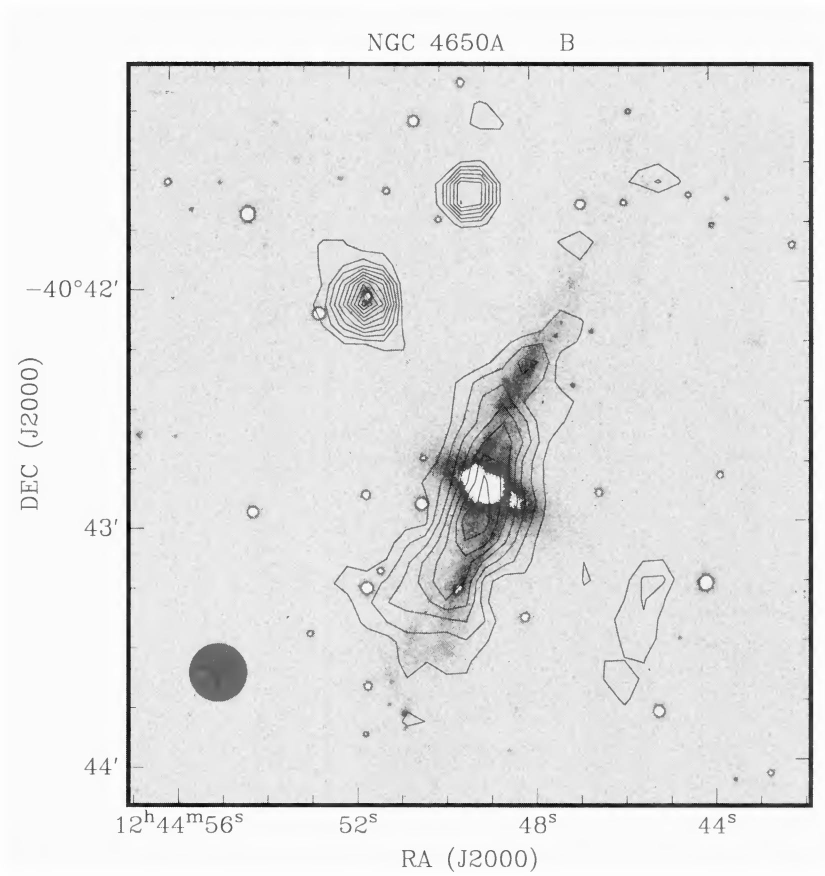

FIG. 6. Continuum map for NGC 4650A. Continuous-lines indicate contours from 0.12 mJy in steps of 0.06 mJy; the beam size is 15″×15″. The continuum emission is stretched along the PR and is possibly linked to star formation occurring in it.

above 2.5 mJy beam^{-1} in this smoothed cube.

2.2 *B*-band Imaging

We obtained a 10 min *B*-band image of NGC 4650A at the ESO NTT in 1996 April, with the ESO Multi-Mode Instrument (EMMI) in the RILD mode and the 2048×2048 Tektronix CCD; the angular scale is 0.27″ per pixel. The seeing during the observations was 1″ FWHM. Dome-flats were obtained during the day and sky-flats at twilight: several sky-flats were obtained to correct for cosmic rays and foreground stars. The image was de-biased and flat-fielded using standard routines in IRAF.

3. RESULTS

The high resolution channel maps for the neutral hydrogen in the polar ring galaxy NGC 4650A are shown in Fig. 1, and the low and high resolution total hydrogen distribution are displayed in Fig. 2 superposed on the Digital Sky Survey (DSS) image. Figure 3 shows the mean velocity field.

With our four-fold increase in velocity resolution and higher sensitivity, our new H I data differ from those previously published by vGSK87, see Table I for a direct comparison. The new ATCA observations show in addition to the H I detected by vGSK87, a faint much more extended H I structure. While the bulk of the H I emission is concentrated in an elongated structure extending out to 2.5′ on each side of the galaxy, we also detect additional filaments and/or detached H I clouds out to 4′ north and south of the galaxy center [Fig. 2(b)]. These structures are most evident in the 40″ resolution map [Fig. 2(a)]: the southern elongation shows up as an arch, attached to the main H I emission, while the northern emission could be loose clouds falling towards the polar ring structure. The total H I flux in the map is 23 Jy km s^{-1}, and corresponds to a total H I mass of 8 $\times$ 10^9 M$_\odot$. This is two times higher than the total mass of 4.6 $\times$ 10^9 M$_\odot$ reported by vGSK87. An H I total flux of 23 Jy km s^{-1} was also found by Richter *et al.* (1994) in their H I survey of polar ring galaxies. We do not find any H I emission in our ATCA data cube at the RC3 velocity for the nearby spiral galaxy NGC 4650 ($v_{\rm sys}$ = 2953 km s^{-1}). We observed NGC 4650A and NGC 4650 with the Parkes 64m telescope on 1996 July 20. The H I profile observed at Parkes is identical to that derived from our ATCA data cube for NGC 4650A and shown in Fig. 4. These observations confirmed the total H I flux detected in our ATCA maps for NGC 4650A, and the single disk H I spectrum at the position of NGC 4650A show no H I other than that of NGC 4650A. No other H I emission was detected in the velocity range 0–7000 km/s.

The high spatial resolution of the new data shows the presence of a barely resolved depletion at the center of the H I distribution. Its size is probably less than 10″, and it coincides with the center of the S0, while vGSK87 find it offset with respect to the galaxy center. We produced a smoothed data cube, with a spatial resolution similar to vGSK87, and the depletion at the center of the H I distribution was still coincident with the galaxy center. The iso-velocity contour of the systematic velocity,[2] $v_{\rm sys} = 2905$ km s^{-1}, coincides with the central depletion in the H I distribution, and is aligned with the S0 minor axis. We do not find the displacement of the systemic velocity contour described by vGSK87. The iso-velocity field contours also show some wiggles where the optical PR crosses in front of the central S0, see Sec. 4.

The inner parts of the H I distribution are very elongated; the projected axis ratio of the H I contours is $b/a \approx 0.16$ which implies a nearly edge-on H I distribution out to ~60″ from the galaxy center, while it becomes more face-on in the outer regions ($b/a \approx 0.38$). The H I intensity map shows several secondary peaks and wiggles in the central distribution, with spatial scales of ~20″, which possibly indicate the presence of self-gravitating structures.

The position-velocity diagrams (PVDs) computed by projecting the data cube onto the major axis of the polar rings are shown in Fig. 5. We adopt the same P.A. for the polar ring major axis as in WMS, i.e., P.A.=158°. Modeling an infinitely narrow ring would produce a linear PVD; the PVD computed by projecting the whole data cube onto the major axis of the polar ring clearly shows that we are looking at H I distribution in a disk, and not in a ring; in this sense, our PVDs in Figs. 5(a), and 5(b) differ from that of vGSK87. [3] In addition to the inner rigid body rotation part plus the outer flattening of the rotation curve, we also see gas at velocities nearer to the systemic velocity, and our PVD looks like that of a rotating gas disk. The PVDs in Figs. 5(a) and 5(b) show also the asymmetry related to the SW arch and its falling velocities. If we assume that the H I is in circular orbits at those distances, the falling velocity can be explained by the presence of H I gas at different inclinations from that of the central edge-on disk.

The velocity field of the outer faint H I looks like the simple continuation of the velocity field of the inner brighter H I, and there seems to be no indication of lower rotation velocities at large radii ~50 kpc.

The continuum map at 20-cm is shown in Fig. 6: the total integrated flux is only 5.4 mJy and the continuum emission is concentrated along the polar ring. It is probably related to the radio-emission due to star formation in the PR. There is continuum emission at the position of SN 1990I, but its flux is too low to get a useful H I absorption spectrum. The other bright continuum sources nearby are NGC 4650 and its very small companion: their total fluxes are 2.4 mJy and 0.3 mJy, respectively.

4. DISCUSSION

The new high resolution H I data, combined with the optical and near-infrared images, allow us to test the proposed models for the polar ring galaxy NGC 4650A. Models for this galaxy should simultaneously account for the morphology of the polar structure in the optical and near-IR, plus the H I distribution and kinematics. Particular points include the location of surface brightness peaks in the NTT B-band image, the peaks in the H I distribution and the structure seen in the K-band image.

As a first step, we discuss published geometries for the PR which were formulated prior to the acquisition of the near-infrared images and the high resolution H I data. S94 proposed a descriptive warp model based on the assumption that the bisymmetric knots seen at ~30″ in the PR B-band image are caused by orbit crowding and superposition, and in rough agreement with the axis ratio of the H I contours of the vGSK87 data at large radii, as they state in S94, Sec. *4.1*. They assumed that all H I orbits are polar, but their inclinations to the sky plane vary linearly with galactocentric radius r along the ring major axis such that the orbits are 10° from edge-on at center, edge-on at r=30″, and at −20° from edge-on at r=90″, and have constant line of nodes. To compare the S94 model with our new data, we built up a 3D model cube based on the S94 warp geometry and using concentric massive wires, where we assume arbitrarily that the radial H I density decreases linearly with radius, and adopt the optical rotation curve along the PR major axis (WMS, SS). We include the beam-smearing effects for an accurate comparison with our H I observations. Although we find that the kinematics predicted by the S94 model for the polar ring is quite consistent with the new H I data, it is not consistent with the total H I map. The S94 model for the H I gas in the polar ring produces peaks in the H I intensity distribution at r=30″. They coincide with the optical B-band peaks in the ring and are due to orbit crowding in the warp, while the H I peaks in our data occur at smaller radii, r~10″. In fact, the peaks in our total H I map do not coincide with any peaks in the ring light distribution, arguing that none of them is due to projection effects of the warp. From the ESO NTT image it is also clear that the bright bisymmetric knots in the PR at a distance of 30″ from the galaxy center are point-like; they do not look like emission from extended regions, such as the smooth distribution one would get from the crowding of the orbits through a warp structure. The S94 warp model also does not reproduce the morphology of the PR as it appears in the K-band image of NGC 4650A (Arnaboldi *et al.* 1995). While the S94 model predicts essentially straight H I contours out to r=45″,[4] [see Fig. 7(a)], the K-band image shows an ''S'' shape for the stellar distribution in the polar ring.

Polar ring systems as a class are very dusty (Arnaboldi *et al.* 1995); in order to identify the old stellar population, which contains most of the luminous mass, NIR photometry is needed. Any models for the polar ring in NGC 4650A must account for the morphology of the K-band image, because it traces the bulk of the stellar population in the PR structure. The K-band image seems to indicate the presence of a more severe warp in the PR central regions than that given by the S94 model. We now attempt to reproduce the S-shaped PR K-band morphology using a more elaborate

[2]Here the systemic velocity is computed as the average between the extreme velocities in the H I high resolution data cube.

[3]vGSK87 did not report how wide their slice was in the data cube to produce the PV diagram in their Fig. 9. We assume that they produced the PVD by projecting the whole data cube onto the PR major axis, as they stated in p. 463.

[4]In the S94 warp model the effect of the twisting is more evident at larger radii.

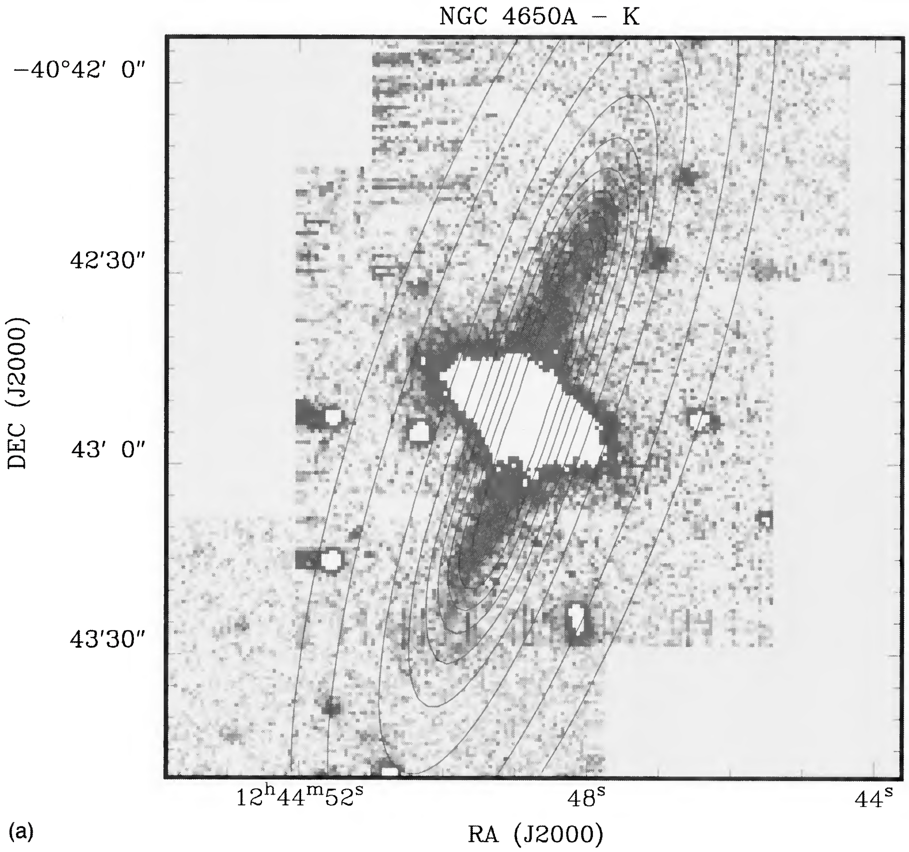

(a)

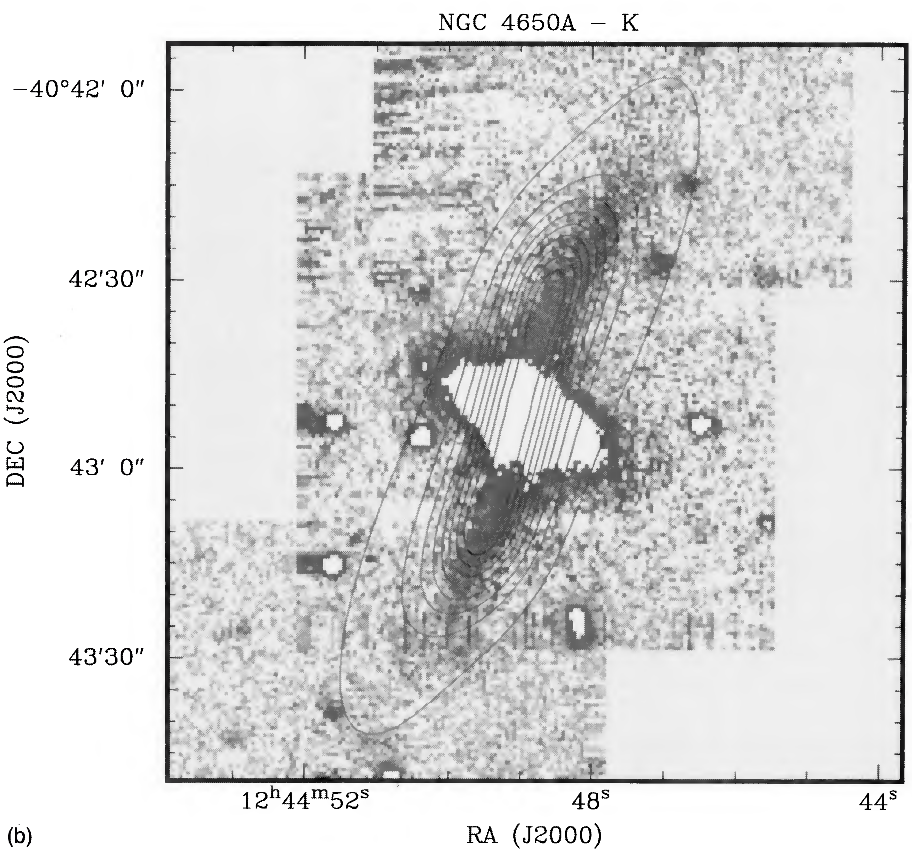

(b)

FIG. 7. (a) Predicted H I distribution from the S94 model superposed on the *K*-band image of NGC 4650A. The contours are straight, while the light indicates an "S" shape. (b) Predicted H I distribution from the more severe warp model, described in the text, superposed on the *K*-band image.

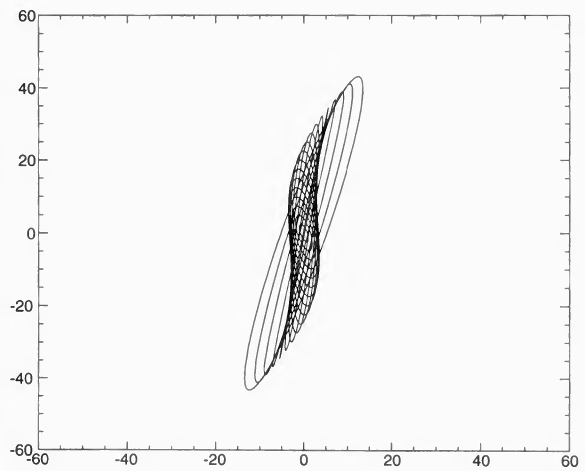

FIG. 8. Best fit warp geometry to the K-band "S" shape of the light in the PR. The scale and the origin of the model is the same as in Fig. 7(b). Units on x,y axes are in arcseconds.

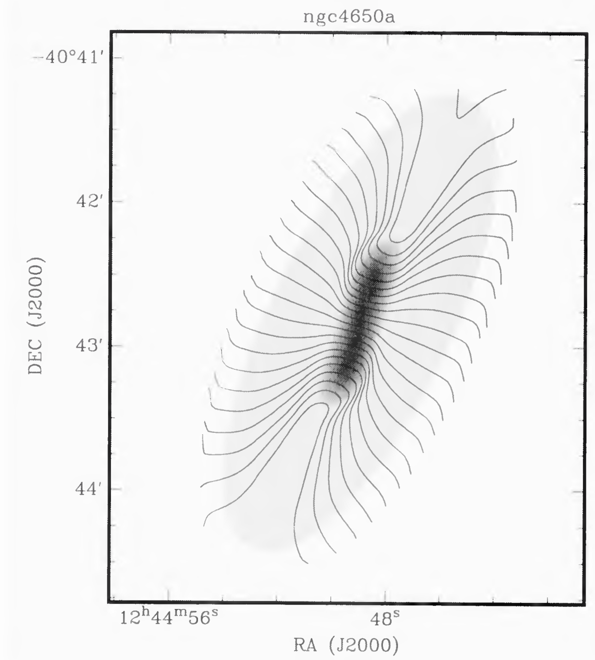

FIG. 9. 2D velocity field computed for the severe warp model described in the text: iso-velocity contours are plotted in step of 10 km s^{-1} on top of the model H I distribution (greyscale). The warp geometry introduces a strong twist in the velocity field, which is clearly different from the butterfly-shape contours expected in a coplanar disk with flat rotation curve. Compare with Fig. 3(a).

warped geometry with orbits that are not precisely polar; an initial guess is derived using the method of Arnaboldi & Galletta (1993), then the 3D data cube is computed as above. The geometry of the warp is tuned till a satisfactory fit to the morphology of the PR in the K-band image is achieved. In the coordinate system of the S0 galaxy, with the xy-plane in the equatorial plane of the S0 and the y-axis towards the observer, we used the usual Euler angles φ, ϕ. We used 30 circular massive wires with $r=0''$ to $r=45''$, with linear variations of φ from 45° to 80° and θ from 80° to 100° (polar orbits correspond to θ=90°). In Fig. 8 we show the warp geometry of the best fit model to the K-band image. This severe warp structure fits the observed PR morphology in the K-band image, but we must now compute the expected H I distribution and velocity field, and compare them with the new H I data. The predicted H I distribution is shown in Fig. 7(b). The predicted velocity field shows a significant twisting of the iso-velocity contours (see Fig. 9) which is inconsistent with the regular observed 2D velocity field for the PR in NGC 4650A, seen in Fig. 3. The velocity field of this warp model is similar in character to that of, e.g., NGC 660 (van Driel *et al.* 1995; Arnaboldi & Galletta 1993), while the 2D H I velocity field for the PR in NGC 4650A is fairly regular, and indeed very similar to the one expected for an edge-on disk which becomes more face-on only at larger radii.

To understand whether the observed H I distribution was indeed following the light in the PR, we compared the high resolution H I maps with the ESO NTT B-band image. To do so, we used foreground stars in common between this image and the DSS image to define the RA-DEC coordinate system on the NTT image and display the H I contours. When the H I density contours are superimposed on the B-band image [Fig. 10(a)] (Plate 19), we see that the H I peaks do not coincide with light peaks in the ring, and occur at minima in the light distribution. If NGC 4650A has the usual dust-to-gas ratio, then this suggests that these minima are due to absorption by a dust lane, and it implies that the optical morphology of the polar ring is probably due to absorption and star forming regions and is not caused by projection effects of a warped structure. In principle, the H I peaks that we see in projection coincident with the dust may come from larger radii, and be related to a very irregular and clumpy H I distribution. However the kinematics of this gas shows that its velocities are at the peak of the rotation curve, and it indicates that this gas must be at small radii, and it spatially coincides with the dust. In addition, where the PR is clearly seen in front of the S0, we see perturbations in the iso-velocity contours [see Fig. 10(b)], and no peak in the H I surface density, while a severe warp model would predict a peak in the H I distribution at this location.

The B-band image [Figs. 10(a) and 10(b)] show a clear dust lane stretching along the major axis of the PR. An unsharp-masked version of this image shows that this dust lane continues inward from 30″ NW to within 1.3″ NE of the nucleus; it reappears 1.3″ SW of the nucleus and reaches out to about 30″ to the SE. This indicates clearly that the polar structure extends continuously to within about 200 pc of the nucleus of the S0. There is no indication of a central hole in the optical component in the PR.

In summary, the K-band image and our new B-band image and H I observations are inconsistent with the warps models for the stars and gas in the polar ring. The more sophisticated warp model described above is also not adequate to explain the optical and near-IR morphology and the properties of the H I data cube for the polar ring of NGC 4650A.

We suggest that a better explanation for all the data is given by the presence of spiral arms in the polar structure. In NGC 4650A the PR surface mass density in gas and stars within a radius of 60″=11 kpc is high enough to maintain a self gravitating spiral pattern. A lower limit for the stellar

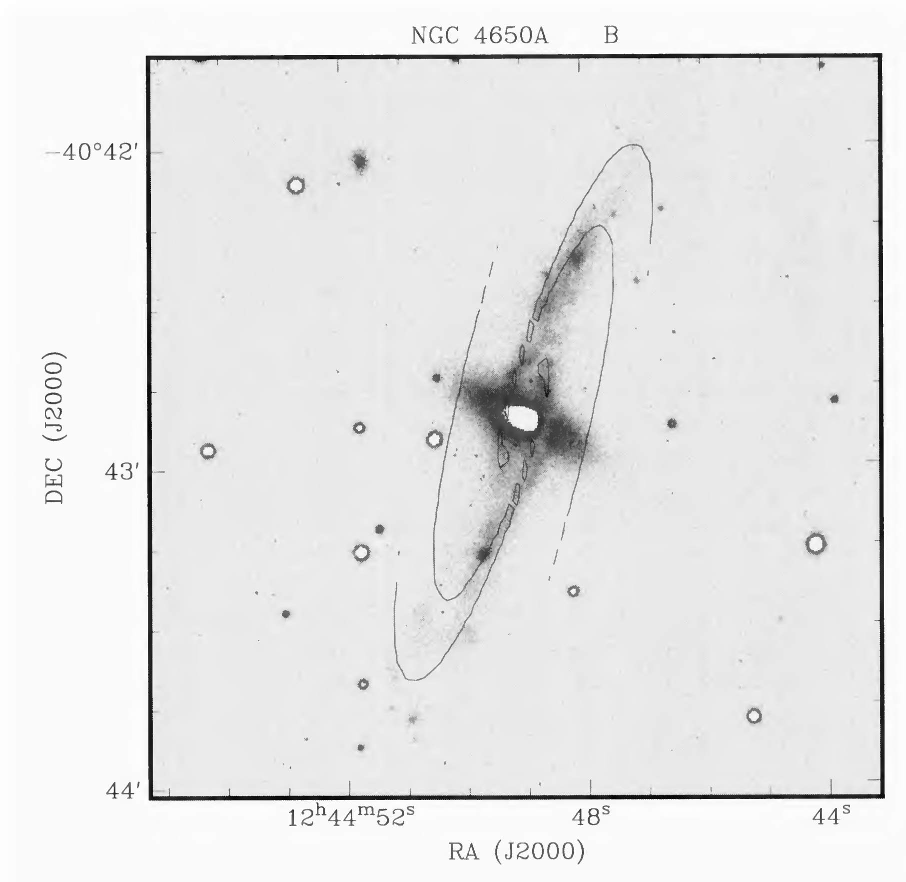

FIG. 11. Spiral arms model for the polar structure in NGC 4650A.

surface density $\Sigma_{\rm star}$[5] is 24 $M_\odot$ pc^{-2}, while a lower limit to the H I surface mass density, once we account for the inclination effects, is 3.5 $M_\odot$ pc^{-2}; the total surface mass density amounts to $\Sigma_{\rm total}$ = 27.5 $M_\odot$ pc^{-2}. The radial wavelength of the self-gravitating spiral pattern will be close to the maximum unstable wavelength

$$\lambda_{\rm crit}=\frac{4\pi G\Sigma_{\rm total}}{\kappa^2},$$

where κ is the epicyclic frequency. If we assume a flat rotation curve, then $r\kappa(r) = \sqrt{2} \times 120$ km s^{-1}, and setting r=10 kpc we obtain $\lambda_{\rm crit} \approx 5$ kpc = 26″. This radial wavelength corresponds to an open spiral arm pattern like the one we fit to the PR in NGC 4650A in Fig. 11. These spiral arms are computed for a logarithmic spiral density distribution with a 25° pitch angle, which crosses the major axis of the polar disk on the sky at 195″ from the polar disk center. We have assumed a constant inclination for the polar disk of 80°.

We suggest that spiral arms seen in projection are responsible for the "S" shape in the K-band image, for the dust lanes, and for the bright optical knots and the blue arms in the optical image, as shown in Fig. 11. We note that spiral arms can perturb the H I velocity field in such a way that it deviates from that of a straight coplanar disk as seen in Fig. 10(b). Furthermore, the H I intensity peaks in NGC 4650A occur on the dusty regions, as in the normal spiral M81 (Kaufman *et al.* 1989a; Kaufman *et al.* 1989b).

A very deep image of the field around NGC 4650A kindly given to us by David Malin indeed shows low surface brightness features NW of the PR which follow our proposed spiral arm, see Fig. 12.

5. CONCLUSION

Previous studies of the dynamics of the polar ring galaxy NGC 4650A indicated that high resolution H I observations were crucial to constrain the dynamical parameters of this system. These observations were carried out at the ATCA, and the results of the analysis indeed confirmed such expectations. The new high resolution H I maps show that the warped geometries proposed so far to explain the optical and near-infrared morphology of NGC 4650A are inconsistent with the hydrogen gas distribution and kinematics. They show that the H I gas is distributed in an almost edge-on disk, which becomes more face-on at larger radii. Comparison of the H I map with a new B-band image obtained in good seeing indicates that H I peaks do not follow peaks in the light, but coincide with absorption features. Therefore a warp geometry will not be able to explain both the optical morphology and the H I distribution in the PR. We do see a warp in the H I distribution at large radii, but it is not related to any optical morphology of the polar structure.

The H I data, and the optical and near-infrared images can be reconciled by the presence of spiral arms in the almost edge-on polar disk. These new observations argue against the

[5]We adopt for the PR stellar component a total mass of 9.5×10^9 $M_\odot$ (Combes & Arnaboldi 1996) and an outer radius of 60″.

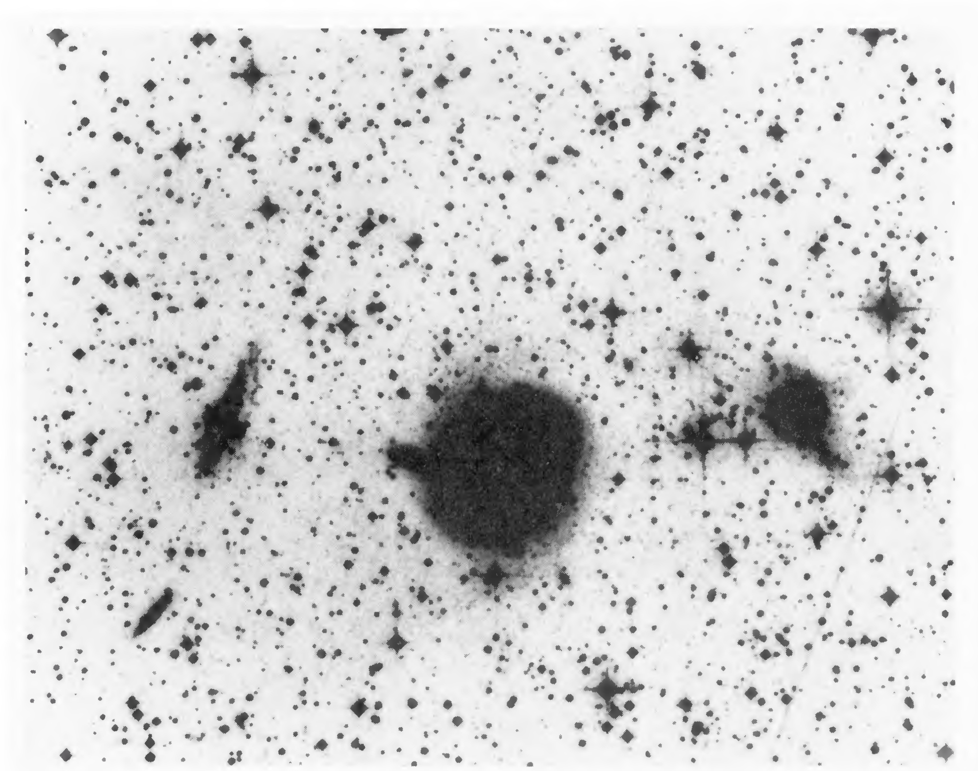

FIG. 12. Negative of a deep image of the NGC 4650 group obtained by David Malin using 7 UKST plates, with emulsion IIIa-J and the GG 395 filter (passband from 395 to 530 nm) for a total integration time of 495 min. North is on top, East to the left. The round central object is NGC 4650, the PR galaxy NGC 4650A is on the left.

basic hypothesis assumed so far in the modeling of the dynamics of NGC 4650A i.e., that the polar structure is a ring and its dynamics are driven by the potential of the mass distribution (luminous+dark) associated with the S0. The presence of spiral arms in the polar structure indicates that it is very massive. These new results do strengthen the relationship between polar ring galaxies and spirals as previously pointed out by Arnaboldi *et al.* (1995) and Combes & Arnaboldi (1996). The scenarios for the formation of such a massive polar disk have serious implications about the nature of the dark matter: for an accretion event to produce such a flat disk, dissipative dark matter might be essential. New simulations of the formation process and new dynamical models for the H I and optical structure and kinematics of NGC 4650A should be done, in the light of these new data.

The authors would like to thank the referee whose comments and suggestions greatly improved the presentation of this paper. We would like to thank P. D. Sackett and L. S. Sparke for their comments and suggestions on the preliminary versions of this paper. We would like to thank J. van Gorkom, P. Schecter, and F. Schweizer for very helpful discussions, and R. Sancisi for his suggestion to test the presence of the H I peaks at small radii via their kinematics. It is a pleasure to thank David Malin who kindly sent us the deep image of the NGC 4650 field.

REFERENCES

Arnaboldi, M., Capaccioli, M., Cappellaro, E., Held, E. V., & Sparke, L. 1993 A&A, 267, 21

Arnaboldi, M., Freeman, K. C., Sackett, P. D., Sparke, L. S., & Capaccioli, M. 1995, Planet. Space Sci., 43, 1377

Arnaboldi, M., & Galletta, G. 1993, A&A, 268, 411

Bosma, A. 1981, ANJ, 86, 1971

Briggs, D. S. 1995, BAAS, 187, 112

Carignan, C., & Freeman, K. C. 1988, ApJ, 332, L33

Combes, F., & Arnaboldi, M. 1996, A&A, 305, 763

de Jong, R. S., & van der Kruit, P. C. 1994, A&AS, 106, 451

Freeman, K. C. 1993, in Physics of Nearby Galaxies: Nature or Nurture?, edited by T. X. Thuan, C. Balkowski, and J. T. T. Van (Editions Frontières, Gif-sur-Yvett), p. 201

Kaufman, M., *et al.* 1989a, ApJ, 345, 674

Kaufman, M., Elmegreen, D. M., & Bash, F. N. 1989b, ApJ, 345, 697

Kent, S. M. 1992, in Morphological and Physical Classification of Galaxies, edited by G. Longo, M. Capaccioli, and G. Busarello (Kluwer, Dordrecht), p. 153

Kent, S. M. 1987, AJ, 93, 816

Kent, S. M. 1986, AJ, 91, 1301

Laustsen, S., & West, R. M. 1980, JA&A, 1, 177

Nicholson, R. A. 1989, Ph.D. thesis, Sussex University, UK

Pfenniger, D., Combes, F., & Martinet, L. 1994, A&A, 285, 79

Pfenniger, D., & Combes, F. 1994, A&A, 285, 94

Reshetnikov, V. P., & Combes, F. 1994, A&A, 291, 57

Richter, O. G., Sackett, P. D., & Sparke, L. S. 1994, AJ, 107, 99

Sackett, P. D., & Sparke, L. S. 1990, ApJ, 361, 408 (SS)

Sackett, P. D., Rix, H.-W., Jarvis, B. J., & Freeman, K. C. 1994, ApJ, 436, 629 (S94)

Sault, R. J., Tenben, P. J., & Wright, M. C. H. 1995, in Astronomical Data Analysis Software and Systems IV, ASP Conf. Ser 77, edited by R. A. Shaw, H. E. Payne, and J. J. E. Haynes (ASP, San Francisco), p. 33

Schweizer, F., Whitmore, B. C., & Rubin, V. C. 1983, AJ, 88, 909
van Driel, W., *et al.* 1995, AJ, 109, 943
van Gorkom, J. H., Schechter, P. L., & Kristian, J. 1987, ApJ, 314, 457 (vGSK87)
van der Hulst, J. M., Terlouw, J. P., Begeman, K., Zwitser, W., & Roelfsema, P. R. 1992, in Astronomical Data Analysis Software and Systems I, ASP Conf. Ser. 25, edited by D. M. Worall, C. Biemesderfer, and J. Barnes (ASP, San Francisco), p. 131
Whitmore, B. C., McElroy, D. B., & Schweizer, F. 1987, ApJ, 314, 439 (WMS)

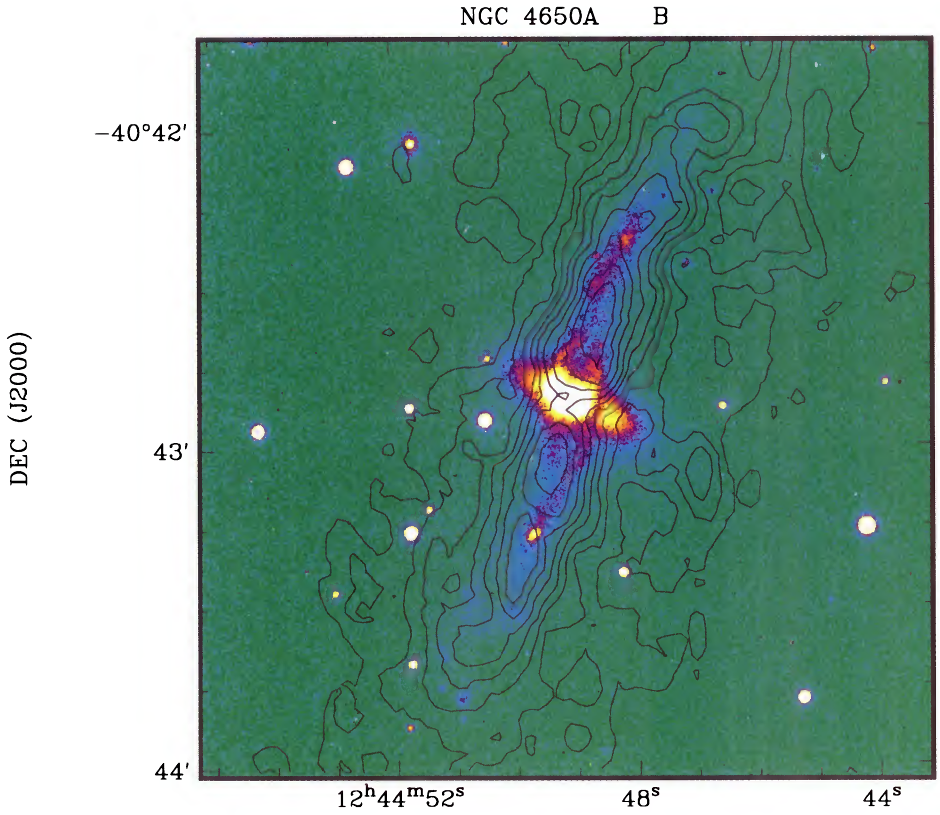

(a)

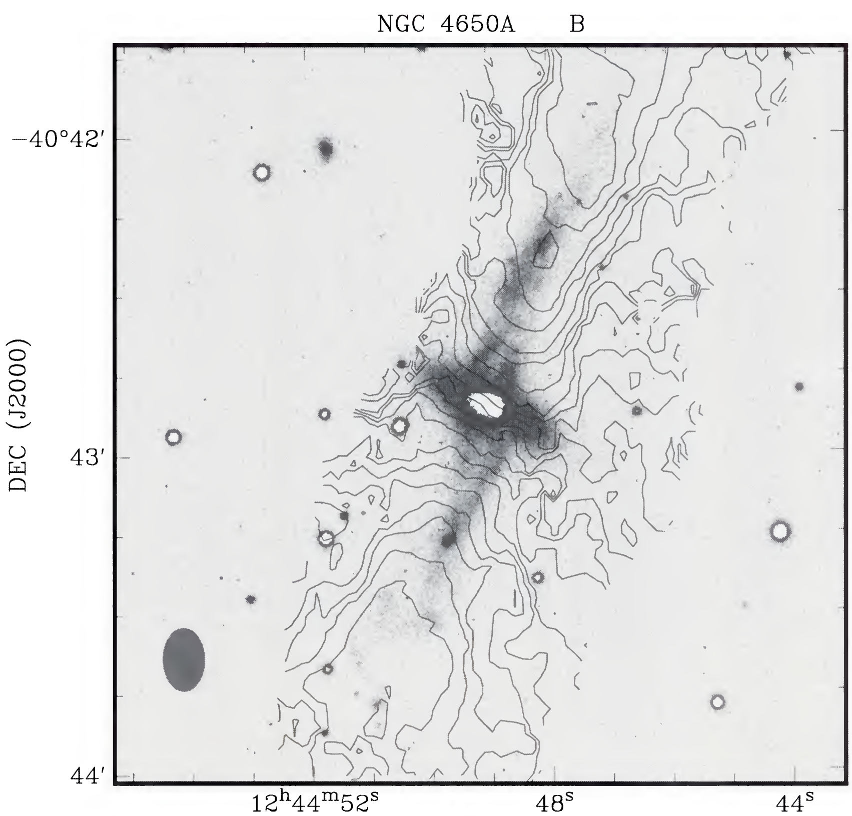

(b)

FIG. 10. (a) H I distribution as in Fig. 2(b) superposed on the ESO NTT B-band image. The peaks in the hydrogen gas distribution lie on top of the absorption feature in the polar structure. (b) H I velocity field as in Fig. 3(b) superposed on the ESO NTT B-band image. Where the polar structure is clearly seen in front of the S0 there are perturbations in the velocity contours, and no peak in the H I distribution.

Arnaboldi *et al.* (see page 595)

THE ASTRONOMICAL JOURNAL

FOUNDED BY B. A. GOULD
1849

VOLUME 113 February 1997~No. 1694 NUMBER 2

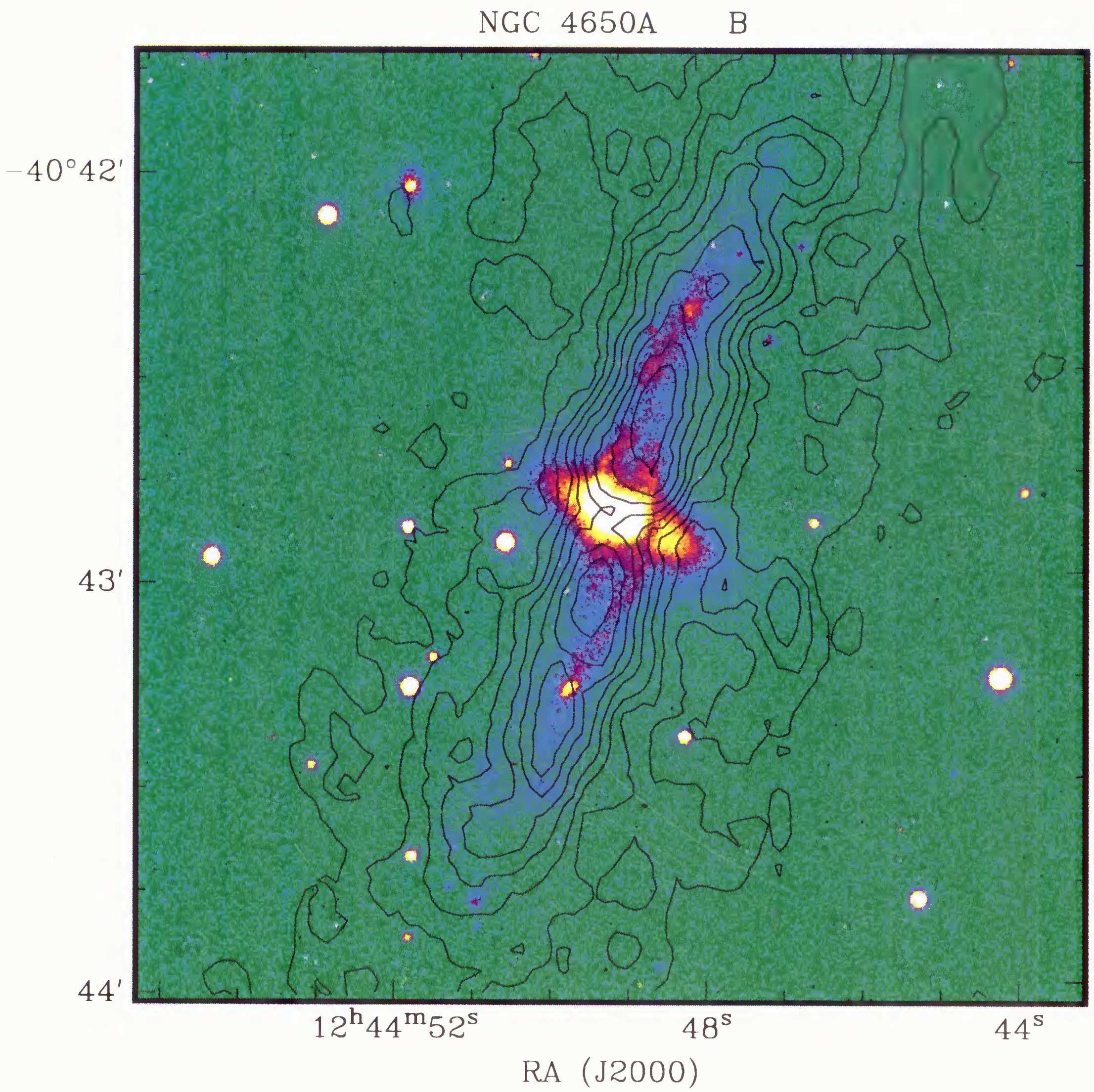

(See Page 585)

Published for the
AMERICAN ASTRONOMICAL SOCIETY
by the
AMERICAN INSTITUTE OF PHYSICS